Hindawi
Journal of Spectroscopy
Volume 2023, Article ID 2393285, 5 pages
https://doi.org/10.1155/2023/2393285

Research Article

The Ultraviolet-Visible Luminescence of Ce^{3+} in $Ca_2Mg(BO_3)_2$ Phosphors with Potential Applications

Jing-Xiang Zhang, Yanru Lin, and Huihong Lin

School of Chemical and Environmental Engineering, Hanshan Normal University, Chaozhou, Guangdong 521041, China

Correspondence should be addressed to Huihong Lin; linhh@hstc.edu.cn

Received 2 March 2023; Revised 6 April 2023; Accepted 12 April 2023; Published 19 April 2023

Academic Editor: Javier Garcia Guinea

New phosphors $Ca_2Mg(BO_3)_2$: Ce^{3+} were synthesized by the solid-state reaction method at a high temperature. The phase purity was characterized by powder X-ray diffraction (XRD). The ultraviolet-visible (UV-Vis) optical properties of Ce^{3+} have been investigated, and the lowest 5d levels, the emission, and the Stokes shifts of Ce^{3+} in the host lattice were identified. In addition, its concentration quenching process was also studied. The results show that Ce^{3+} ions enter Ca^{2+} sites with only one emission in a UV-Vis range and that the optimum doping concentration is $x = 0.05$. The excitation and emission spectra were evaluated to clearly reveal luminescence features.

1. Introduction

Rare earth ion-doped borates were extensively studied because of their excellent luminescent properties and wide applications, such as SrB_4O_7: Eu in UV-emitting medical lamps, $GdMgB_5O_{10}$:Ce^{3+}, Tb^{3+} as a green component of tricolor lamps, and (Y, Gd)BO_3:Eu^{3+} as a red phosphor in plasma display panel devices (PDPs) [1, 2].

Trivalence cerium ions (Ce^{3+}) have $4f^1$ configurations, and Ce^{3+} activated inorganic luminescent materials can realize the ultraviolet to red emission due to the host-dependent 4f-5d transition luminescence characteristics of Ce^{3+} [3–7], which makes Ce^{3+} activated phosphors significant candidates for pc-LEDs. Because the f-d transitions of Ce^{3+} are partly allowed, they have large absorption cross-sections and appear as intense bands in spectra, and hence, luminescent materials doped with Ce^{3+} absorb the excitation energy efficiently. The most famous is $Y_3Al_5O_{12}$: Ce^{3+}, and it can absorb blue light and converts it with high efficiency into yellow emission. The phosphor is now widely used as the yellow component in GaN-based white-emitting LEDs (light-emitting diodes) [8–12].

Ce^{3+} has the $4f^1$ ground-state configuration with the first excited states belonging to the 5d configuration. The excitation spectrum of Ce^{3+}5d-4f emission provides information on the crystal-field splitting and the centroid energy of the 5d states in a host lattice. Similar crystal-field splitting is expected for all lanthanide ions in the same host lattice. That is, when the 5d level energies of Ce^{3+} are known in a specific host lattice, they can be used to predict the 5d states for the other lanthanide ions in that same lattice. The investigation of the spectroscopic properties of Ce^{3+} in different host lattices is then important not only for possible application but also for basic research.

In 1974, Verstegen first reported the luminescence of Tb^{3+} in $X_2Z(BO_3)_2$ (X = Ba, Sr; Z = Ca, Mg) [13]. It is reported that $Ca_2Mg(BO_3)_2$ is tetragonal and that $Ba_2Mg(BO_3)_2$ is hexagonal and isomorphous with the mineral buetschliite. $Ba_2Ca(BO_3)_2$ and $Sr_2Mg(BO_3)_2$ are related to buetschliite, but their diffraction patterns point to a crystallographic system of lower symmetry [14, 15]. As a series of borates with relevant composition and structure, a comparison of Ce^{3+} luminescence properties in $Ba_2Mg(BO_3)_2$, $Ba_2Ca(BO_3)_2$, and $Sr_2Mg(BO_3)_2$ was conducted in our present work [16–20]. Ce^{3+} in isomorphic $Ba_2Ca(BO_3)_2$ and $Sr_2Mg(BO_3)_2$ showed similar excitation spectroscopic properties but was different from that in $Ba_2Mg(BO_3)_2$. Because of the different coordination polyhedrons, Ce^{3+} ions in former two hosts showed larger crystal-

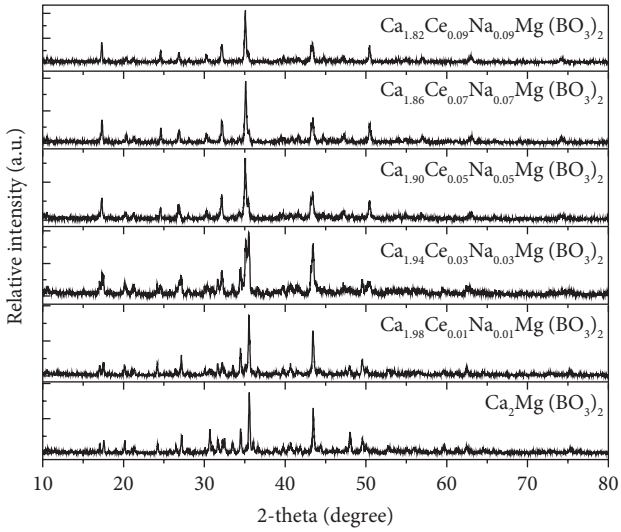

Figure 1: XRD patterns of $Ca_{2(1-x)}Ce_xNa_xMg(BO_3)_2$ ($x = 0$, 0.01, 0.03, 0.05, 0.07, and 0.09).

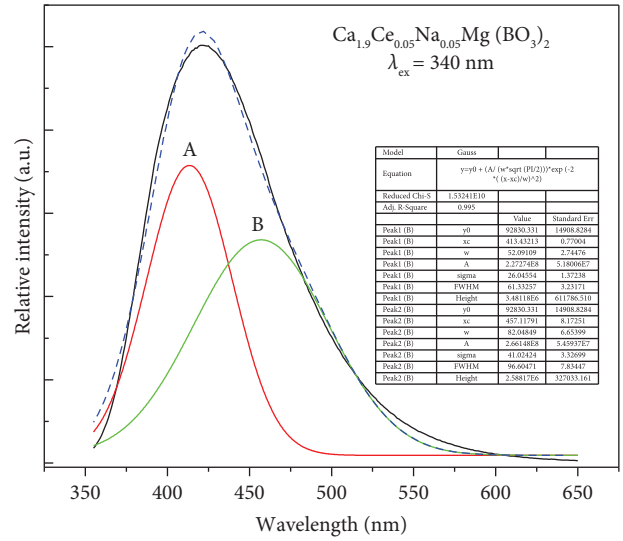

Model	Gauss		
Equation	y=y0 + (A/ (w*sqrt (PI/2)))*exp (-2 *((x-xc)/w)^2)		
Reduced Chi-S	1.53241E10		
Adj. R-Square	0.995		
		Value	Standard Err
Peak1 (B)	y0	92830.331	14908.8284
Peak1 (B)	xc	413.43213	0.77004
Peak1 (B)	w	52.09109	2.74476
Peak1 (B)	A	2.2727e8	5.18006E7
Peak1 (B)	sigma	26.04554	1.37238
Peak1 (B)	FWHM	61.33257	3.23171
Peak1 (B)	Height	3.4811E6	611786.510
Peak2 (B)	y0	92830.331	14908.8284
Peak2 (B)	xc	457.11791	8.17251
Peak2 (B)	w	82.04849	6.65399
Peak2 (B)	A	2.6614e8	5.45937E7
Peak2 (B)	sigma	41.02424	3.32699
Peak2 (B)	FWHM	96.60471	7.83447
Peak2 (B)	Height	2.5881E6	327033.161

Figure 2: UV-Vis emission spectra of $Ca_{1.9}Ce_{0.05}Na_{0.05}Mg(BO_3)_2$ at RT.

field splitting values. Owing to stronger electron-lattice interaction, the Stokes shift was larger for Ce^{3+} in $Ba_2Mg(BO_3)_2$. To fully present Ce^{3+} luminescence in borates $X_2Z(BO_3)_2$ (X = Ba, Sr, Ca; Z = Ca, Mg), here, we have reported Ce^{3+} luminescence properties in another borate $Ca_2Mg(BO_3)_2$.

2. Materials and Methods

The samples were prepared by a solid-state reaction route at a high temperature. The reactants include analytical grade pure $CaCO_3$ (AR), MgO (AR), and H_3BO_3 (AR, excess 3 mol % to compensate evaporation), and 99.95% pure rare-earth oxide CeO_2 and Na_2CO_3 (AR) were added as charge compensators in all rare-earth doped samples. According to the nominal compositions of compounds, an appropriate amount of starting materials was thoroughly mixed and ground, and subsequently, the mixture was prefired at 500°C for 1 h. After milling for a second time, the samples were calcined at 950°C for 6 h in a CO-reducing atmosphere. After these steps, the temperature was slowly cooled down to room temperature.

The structure of the final products was examined by X-ray powder diffraction (XRD) using Cu Kα radiation on a RIGAKU D/max 2200 vpc X-ray diffractometer with 40 kV, 30 mA. The UV excitation and emission spectra of the phosphors were recorded on an EDINBURGH FLS 920 spectrofluorometer at room temperature, and a 450 W xenon lamp was used as an excitation source.

3. Results and Discussion

3.1. Powder X-Ray Diffraction (XRD). The measurements on powder X-ray diffraction for all samples were performed to verify the phase purity and to check the crystal structure. The XRD patterns of samples $Ca_{2(1-x)}Ce_xNa_xMg(BO_3)_2$ ($x = 0$, 0.01, 0.03, 0.05, 0.07, and 0.09) are presented in Figure 1. The results show that all Ce^{3+}ion-doped samples in the investigated concentration range are also of a single phase, which are also in line with an undoped sample $Ca_2Mg(BO_3)_2$, and the crystal structure is not significantly changed when the doped ions enter into the host and occupy Ca^{2+} normal sites. It is reported that $Ca_2Mg(BO_3)_2$ was isomorphous with $Na_2Ca(CO_3)_2$ and tetragonal with $a = 5.14$ Å and $c = 4.41$ Å [13]. According to the effective ionic radii and identical valence, Ce^{3+} will mainly enter the Ca^{2+} sites.

3.2. The UV-Vis Luminescence Properties of $Ca_2Mg(BO_3)_2$: Ce^{3+}. A series of phosphors $Ca_{2(1-x)}Ce_xNa_xMg(BO_3)_2$ ($x = 0.01$, 0.03, 0.05, 0.07, 0.09) were measured. As an example, the emission spectra of $Ca_{2(1-x)}Ce_xNa_xMg(BO_3)_2$ ($x = 0.05$) at 340 nm excitation at RT are illustrated in Figure 2. Under 340 nm UV light excitation, a broad emission band peaking at ~422 nm can be detected, marked as curve a. Usually, Ce^{3+} ions in one specific lattice site will show two emission bands corresponding to the transitions from the lowest 5d excited state to the $^2F_{5/2}$ and $^2F_{7/2}$spin-orbit split 4f ground states. The energy separation of the two emission bands coincides with the spin-orbit splitting and amounts about 2,000 cm^{-1} [5]. Often the two bands are resolved much better at lower temperatures than at room temperature due to a decrease in the electron-lattice phonon interaction.

To determine the emission peak positions for Ce^{3+}, emission spectrum a was fitted with two Gaussian profiles located at about 413 (A) and 457 nm (B). The energy difference is 2331 cm^{-1}, which is slightly larger than the expected value of 2000 cm^{-1} between $^2F_{5/2}$ and $^2F_{7/2}$ of Ce^{3+}. It may be caused by the weak influence of the nephelauxetic effect in the structure. The full width at half maxima (FWHM) of Ce^{3+} emission is estimated to be ~91 nm.

Since the energy difference between band A and B approaches with the the $^2F_{5/2}$ and $^2F_{7/2}$spin-orbit splittings, which are attributed to the emission from Ce^{3+} at one specific site, that is to say, there is only one Ca site in

$Ca_2Mg(BO_3)_2$, similar to $Ba_2Mg(BO_3)_2$, $Ba_2Ca(BO_3)_2$, and $Sr_2Mg(BO_3)_2$ structures. When the Ce^{3+} ion is incorporated in $Ca_2Mg(BO_3)_2$, it may substitute for Ca^{2+}. We have added Na^+ as a charge compensator during synthesis, so the emission of Ce^{3+} in $Ca_2Mg(BO_3)_2$: Ce^{3+} will be associated with charge-compensated Ce^{3+} centers. When Ce^{3+} enters one specific type of Ca^{2+} sites, the doped compound will show only one center emission. In addition, we might also take into account that borate samples are partially hygroscopic, and consequently, the effect of UV exposure (due to the Xe lamp) could induce the radiolysis of the adsorbed water molecules, where the hydroxyl groups can be weakly bonded to cations; these OH- ions are released due to the increase in the temperature or illumination. This interesting effect has been observed in the glow emission of many different materials, which may also be one of the inevitable influencing factors on the UV-green emission from insulator solids [21, 22].

The UV excitation spectra of $Ca_{1.9}Ce_{0.05}Na_{0.05}Mg(BO_3)_2$ under different monitoring wavelengths are displayed in Figure 3, marked as curves *a*, *b*, *c*, and *d*, respectively. Curves *a*, *b*, *c*, and *d* are similar in the range of 250–450 nm. Three broad bands labeled A (~274 nm), B (~309 nm), and C (~340 nm) are clearly observed, and we consider that these bands are mainly associated with the crystal-field split 5d states of Ce^{3+} in the host lattice. As we all know, no extra line or band caused by the interactions of f-f or f-d electrons occurred in Ce^{3+} excitation spectrum, which directly exhibits the information on the crystal-field splitting of the 5d states. The $5d^1$ electronic configuration can be split into 2–5 components by the crystal field, such as bands A, B, and C in Figure 3. Here, we can estimate the lowest f-d transition($5d^1$) absorption of Ce^{3+} locating at ~340 nm (band C: ~29 412 cm^{-1}). Though the spin-orbit splitting doublet emission was not well resolved at RT, we can estimate the Stokes shift (from 340 to 413 nm) to be ~5199 cm^{-1}. Because the Stokes shift is fairly small, obvious spectral overlap is observed between excitation and emission spectra, which directly shows that the energy transfer between neighbor Ce^{3+} is efficient.

Figure 4 shows the emission spectra of $Ca_{1.9}Ce_{0.05}Na_{0.05}Mg(BO_3)_2$ under 254, 309, 340, and 370 nm excitation wavelengths. In Figure 3, we can see these bands were ascribed to the f-d transition absorption of Ce^{3+} in $Ca_2Mg(BO_3)_2$. It can be observed that these emission spectra are almost similar in shape, except for slightly red shifts at 309 and 370 nm excitation. This means that, no matter which wavelength is excited, only the emission from one lattice site can be observed, which is consistent with the above discussion.

Figure 5 presents the emission spectra of $Ca_{2(1-x)}Ce_xNa_xMg(BO_3)_2$ ($x = 0.01, 0.03, 0.05, 0.07, 0.09$) samples at 340 nm excitation. All the emission spectra are very similar in shape, the emission intensity first increases and then decreases regularly, and the optimal emission intensity occurs at $x \approx 0.01$–0.09. The decline of the emission intensity may be ascribed to the concentration quenching effect. In Figure 6, the concentration quenching curve of Ce^{3+} emission at 340 nm excitation is plotted. It can be found that the emission intensity of Ce^{3+} first increases with an increase

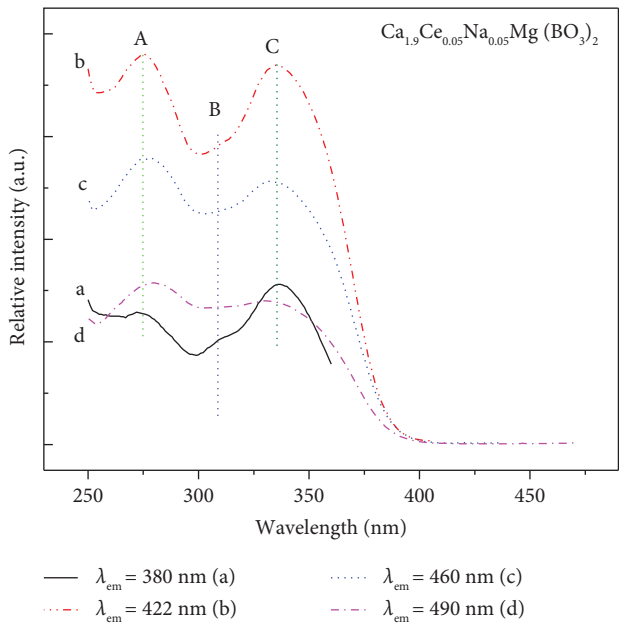

Figure 3: UV excitation spectra of $Ca_{1.9}Ce_{0.05}Na_{0.05}Mg(BO_3)_2$ at RT.

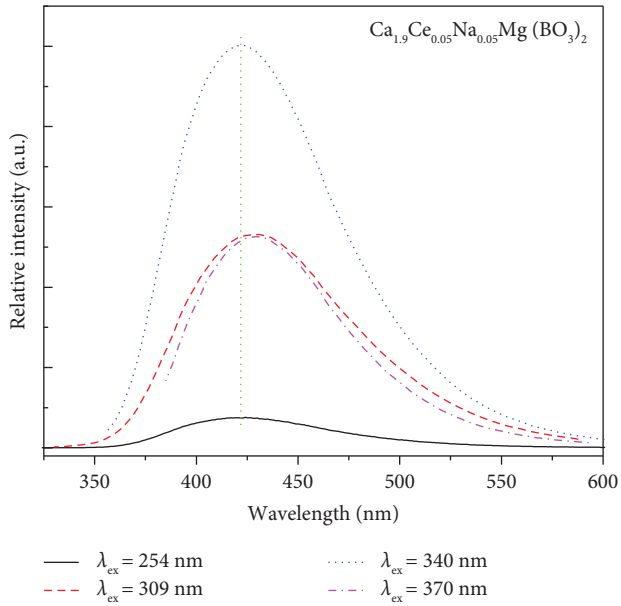

Figure 4: The emission spectra of $Ca_{1.9}Ce_{0.05}Na_{0.05}Mg(BO_3)_2$ under different excitation wavelengths at RT.

in Ce^{3+} concentrations (x), reaching a maximum around $x = 0.05$, and then decreases with an increasing concentration due to concentration quenching.

Based on the optimal Ce^{3+} doping concentration, the crucial energy transfer distance (R_c) among Ce^{3+} ions in the $Ca_2Mg(BO_3)_2$ host can be calculated using the following equation (23):

$$R_c \approx 2\left(\frac{3V}{4\pi x_c N}\right)^{1/3}, \quad (1)$$

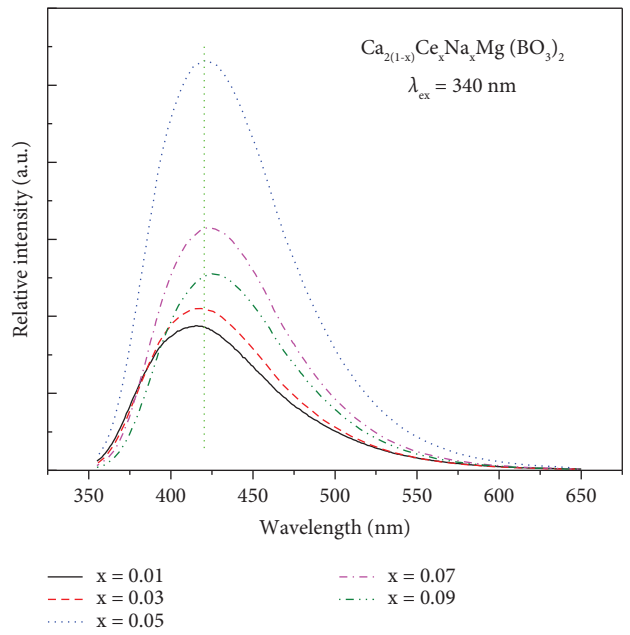

Figure 5: The emission spectra of $Ca_{2(1-x)}Ce_xNa_xMg(BO_3)_2$ ($x = 0.01$, 0.03, 0.05, 0.07, and 0.09) samples with $\lambda_{ex} = 340$ nm.

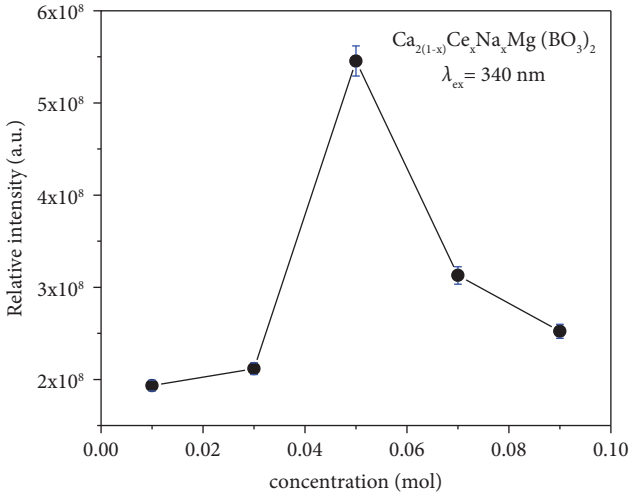

Figure 6: The emission intensities of Ce^{3+} as a function of its doping concentration (x) in $Ca_{2(1-x)}Ce_xNa_xMg(BO_3)_2$ samples at RT.

where V is the cell volume, N is the number of cations which were substituted by Ce^{3+} ions in the unit cell, and x_c is the optimal doping concentration. In present case, $V = 320.5$ Å^3, $N = 4$ (for Ca sites), and $x_c = 0.05$. Therefore, the crucial energy transfer distance can be estimated as 8 Å. The determined R_c value is slightly larger than 5 Å, indicating that multipolar interactions are dominant for the concentration quenching of Ce^{3+}.

4. Conclusions

The spectroscopic properties of phosphors $Ca_2Mg(BO_3)_2$: Ce^{3+} in UV-Vis ranges were investigated. The lowest 5d state of Ce^{3+} in $Ca_2Mg(BO_3)_2$ was observed at 340 nm, and the Stokes shift was estimated to be ~5199 cm^{-1}. A wider broad band from 350 to 600 nm emission peaking at 413 and 457 nm was obtained. These information gives us a good idea that Ce^{3+} is a good sensitizer to the other doping ions in $Ca_2Mg(BO_3)_2$, such as Cr^{3+}, Eu^{3+}, Tb^{3+}, Tm^{3+}, and Nd^{3+}. It should be noted it could broaden the emission wavelength range of a phosphor by codoping of Ce^{3+} and other doped ions in the $Ca_2Mg(BO_3)_2$ host lattice; then, potential multifunctional applications will be realized.

Data Availability

The data used to support the findings of this study are included within the article.

Conflicts of Interest

The authors declare that they have no conflicts of interest.

Acknowledgments

This work was supported by the Guangdong Basic and Applied Basic Research Foundation (Nos. 2021A1515012358 and 2020A1515011403), the Innovation Team Program of Higher Education of Guangdong, China (2017KCXTD023), the Hanshan Normal University Start-Up Fund for Professor Scientific Research (QD202203), and the University-Enterprise Collaborative Innovation Center for Big Health Industry (2022 Hybribio Special Project, 0002/b22088).

References

[1] G. Blasse and B. C. Grabmaier, *Luminescent Materials*, Springer-Verlag Press, Berlin, Germany, 1994.

[2] S. Shionoga and W. M. Yen, *Phosphor Handbook*, CRC Press, Boston, MA, USA, 1999.

[3] L. van Pieterson, M. F. Reid, R. T. Wegh, S. Soverna, and A. Meijerink, "4fn⟶4fn-15d transitions of the light lanthanides: experiment and theory," *Physical Review B*, vol. 65, no. 4, Article ID 045113, 2002.

[4] P. Dorenbos, "5d-level energies of Ce^{3+} and the crystalline environment I. Fluoide compounds," *Physical Review B*, vol. 62, no. 23, pp. 15640–15649, 2000.

[5] P. Dorenbos, "5d-level energies of Ce^{3+} and the crystalline environment. III. Oxides containing ionic complexes," *Physical Review B*, vol. 64, no. 12, Article ID 125117, 2001.

[6] T. Jüstel, H. Nikol, and C. Ronda, "New developments in the field of luminescent materials for lighting and displays," *Angewandte Chemie, International Edition*, vol. 37, no. 22, pp. 3084–3103, 1998.

[7] H. Lin, B. Wang, Q. Huang et al., "$Lu_2CaMg_2(Si_{1-x}Ge_x)_3O_{12}$: Ce^{3+}Solid-solution phosphors: bandgap engineering for blue-light activated afterglow applicable to AC-LED," *Journal of Materials Chemistry C*, vol. 4, no. 43, pp. 10329–10338, 2016.

[8] Q. Peng, C. Liu, D. Hou et al., "Luminescence of Ce^{3+} doped $MB_2Si_2O_8$ (M = Sr, Ba): a deeper insight into the effects of electronic structure and Stokes shift," *Journal of Physical Chemistry C*, vol. 120, no. 1, pp. 569–580, 2016.

[9] T. Hasegawa, S. W. Kim, T. Ueda et al., "Unusual, broad red emission of novel Ce^{3+} activated $Sr_3Sc_4O_9$ phosphors under

visible-light excitation," *Journal of Materials Chemistry C*, vol. 5, no. 36, pp. 9472–9478, 2017.

[10] Z. Song and Q. Liu, "Understanding the abnormal lack of spectral shift with cation substitution in highly efficient phosphor $La_3Si_6N_{11}:Ce^{3+}$," *Physical Chemistry Chemical Physics*, vol. 22, no. 25, pp. 14162–14168, 2020.

[11] F. Su, B. Lou, Y. Ou et al., "VUV-UV-vis luminescence, energy transfer dynamics, and potential applications of Ce^{3+} and Eu^{2+} doped $CaMgSi_2O_6$," *Journal of Physical Chemistry C*, vol. 125, no. 10, pp. 5957–5967, 2021.

[12] D. Hou, R. Huang, J.-Y. Li et al., "Expanded visible-near-infrared temperature sensing properties in view of ultra-broadband tunable luminescence in $Mg_3Y_2Ge_3O_{12}:Ce^{3+}$, Cr^{3+} phosphors with advanced applications," *Journal of Luminescence*, vol. 251, Article ID 119204, 2022.

[13] J. M. P. J. Verstegen, "The luminescence of Tb^{3+} in borates of the composition $X_2Z(BO_3)_2$ (X = Ba, Sr, Ca; Z = Ca, Mg)," *Journal of the Electrochemical Society*, vol. 121, no. 12, p. 1631, 1974.

[14] A. Akella and D. A. Keszler, "Structure and Eu^{2+} luminescence of dibarium magnesium orthoborate," *Materials Research Bulletin*, vol. 30, no. 1, pp. 105–111, 1995.

[15] A. Diaz and D. A. Keszler, "Eu^{2+} luminescence in the borates $X_2Z(BO_3)_2$ (X = Ba, Sr; Z = Mg, Ca)," *Chemistry of Materials*, vol. 9, no. 10, pp. 2071–2077, 1997.

[16] H. H. Lin, H. B. Liang, and B. Han, "Luminescence and site occupancy of Ce^{3+} in $Ba_2Ca(BO_3)_2$," *Physical Review B*, vol. 76, Article ID 035117, 2007.

[17] H. H. Lin, H. B. Liang, Z. Tian et al., "Luminescence of $Ba_2Ca(BO_3)_2$: Ce^{3+}---Influence of charge compensator, energy transfer and LEDs application," *Journal of Physics D Applied Physics*, vol. 42, no. 16, Article ID 165409, 2009.

[18] H. H. Lin, H. B. Liang, G. B. Zhang, and Y. Tao, "A comparison of Ce^{3+} luminescence in $X_2Z(BO_3)_2$ (X = Ba, Sr; Z = Ca, Mg) with relevant composition and structure," *Journal of Rare Earths*, vol. 30, pp. 1–5, 2012.

[19] H. H. Lin, H. B. Liang, Z. Tian et al., "Vacuum-ultraviolet-vis luminescence of dibarium magnesium orthoborate $Ba_2Mg(BO_3)_2$ doped with Ce^{3+} and Eu^{2+} ions," *Journal of Materials Research*, vol. 21, no. 4, pp. 864–869, 2006.

[20] H. B. Liang, H. H. Lin, G. B. Zhang, P. Dorenbos, and Q. Su, "Luminescence of Ce^{3+} and Pr^{3+} doped $Sr_2Mg(BO_3)_2$ under VUV–UV and X-ray excitation," *Journal of Luminescence*, vol. 131, no. 2, pp. 194–198, 2011.

[21] J. Garcia-Guinea, F. Garrido, P. Lopez-Arce, V. Correcher, and J. de la Figuera, "Spectral green cathodoluminescence emission from surfaces of insulators with metal-hydroxyl bonds," *Journal of Luminescence*, vol. 190, pp. 128–135, 2017.

[22] A. Barrera-Villatoro, C. Boronat, T. Rivera-Montalvo, V. Correcher, J. Garcia-Guinea, and J. Zarate-Medina, "Cathodoluminescence response of natural and synthetic lanthanide-rich phosphates (Ln3+: Ce, Nd)," *Radiation Physics and Chemistry*, vol. 141, pp. 271–275, 2017.

[23] H. D. Luo, J. Liu, X. Zheng, L. Han, K. Ren, and X. Yu, "Enhanced photoluminescence of $Sr_3SiO_5:Ce^{3+}$ and tuneable yellow emission of $Sr_3SiO_5:Ce^{3+}$, Eu^{2+} by Al^{3+} charge compensation for W-LEDs," *Journal of Materials Chemistry*, vol. 22, no. 31, pp. 15887–15893, 2012.